An Interactive Platform for a High Performance Digital Twin of a Human Heart

Yujie Gong
Department of Mathematics
University of Macau
Macau, China

Fenfen Qi
Department of Mathematics
University of Macau
Macau, China

Yingzhi Liu
Department of Mathematics
University of Macau
Macau, China

Jing-Yuan Wang
Department of Mathematics
University of Macau
Macau, China

Tianhao Ma
Department of Mathematics
University of Macau
Macau, China

Zaiheng Cheng
Department of Mathematics
University of Macau
Macau, China

Yi Jiang
SIAT
Chinese Academy of Sciences
Shenzhen, Guangdong, China

Rongliang Chen
SIAT
Chinese Academy of Sciences
Shenzhen, Guangdong, China

Xinhong Wang
Department of Radiology
The Second Affiliated Hospital
Zhejiang University School of Medicine
Hangzhou, Zhejiang, China

Li Luo
Department of Mathematics
University of Macau
Macau, China

Xiao-Chuan Cai
Department of Mathematics
University of Macau
Macau, China

***Abstract*—In this paper, we present an interactive platform for visualizing and manipulating the digital twin of a human heart reconstructed from computed tomography (CT). The platform involves a pair of holographical glasses whose cameras are used to input the control parameters by hand gestures, a high-end graphical workstation acting as the platform manager to render the data and control the computations, and a high performance computer cluster which is the workhorse for heavy computations required by the physics-based model of the heart. The numerical model of the heart is referred to as the digital twin of the biological heart, and using the proposed platform we can see and operate on certain part of the heart that is difficult to reach in the biological heart. Such a platform can be used as an off-line tool for surgical planning or as a near real-time tool during the operation. The main focuses of the paper are algorithms and software for manipulating the three-dimensional elastic object through the holographic glasses using hand gestures, the control of the surface geometry, and the near real time computation of the motion and displacement of the elastic body on a parallel computer. The deformation of the heart is modeled by a hyperelasticity equation solved on a supercomputer so that physically meaningful motion is obtained in near real time. Preliminary results are reported for the heart of an actual patient.**

***Index Terms*—Interactive hologram, digital twin, hyperelasticity model of the heart, finite element, domain decomposition, parallel processing**

I. Introduction

In this paper, we introduce an interactive visualization and near real-time manipulation platform for the purpose of surgical planning based on a digital twin of a biological human heart, a holographical device, a graphical workstation, and a supercomputer. Digital twin is a numerical model of the real object with which people can perform different tasks without the cost or potential harm of the object. There are a wide range of applications of this technology. Kang [1] built a digital twin of a bridge in order to monitor the structural health of the bridge during its life time. McClellan [2] constructed a digital twin as a predictive tool to control the landing of an autonomous aerial vehicle. Another digital twin for unmanned aerial vehicle is built by Kapteyn [3] to develop a response plan in case of structural damage or degradation. All the aforementioned techniques are data-based methods. Ritto [4] put forward a digital twin model for damage identification using a physics based model to generate data to train a neural network. In this paper we develop a physics-based model since our object of interests is a heart whose movement and deformation have to satisfy laws of physics represented as a nonlinear system of partial differential equations discretized by a finite element method.

The second component of the platform is a holographic device. Hologram visualization is an important tool in augmented reality (AR) and it provides a way to overlay the digital model on the real object. Many applications are based on the AR technology. Park [5] created a program for CT-guided lesion targeting with which the efficiency for manipulating the procedure is increased and the required dose of radiation is reduced. Hanna [6] applied the AR technology in both clinical and nonclinical applications in pathology that enable the experts to see the operation remotely in real time so that they can offer their advice. Jang et al. [7] tried to view the

The research is supported in part by FDCT 0141/2020/A3, 0079/2021/AFJ, 0090/2022/A2. Y. Gong and F. Qi are the first authors, and L. Luo and X.-C. Cai are the corresponding authors of the paper. Email: liluo@um.edu.mo, xccai@um.edu.mo

979-8-3503-3333-6/23/$31.00 ©2023 IEEE
DOI 10.1109/MetaCom57706.2023.00046

myocardial scar with the hologram to facilitate the surgery. There are also applications for the purpose of education [8] [9] [10] [11] [12]. Sometimes, people are not satisfied with only seeing the object on the AR device. Interaction with the visual is also desired. Mixed reality (MR) allows the user to interact with both the virtual object and the real object. Holograms are used to achieve MR because of its three-dimensional capabilities. Cartucho [13] built a MR visualization platform that projects multiple MRI and CT images to provide real-time guidance to surgeons during the operation. The users can selectively view the medical images by hand gestures.

Predicting the physically correct elastic deformation of an object is important in many engineering and medical applications, such as the structural changes of a bridge in an earthquake [14] and the behavioral changes of the muscles of the human heart [15] under different medical conditions. Traditionally, the deformation is viewed in the form of 2D images or videos on the screen, and in some situations it is not easy to find the changes in the dimension perpendicular to the imaging dimensions. With the hologram technology (or extended reality technology), users are able to view and interact with the visual object directly in 3D and from any desirable angles.

Physics-based digital twin is often computationally more expensive than data-based (image-based) digital twins, but has been attempted by researchers. Lopez [16] proposed a digital twin of a river dam to understand and predict if it works safely under normal and certain extreme situations. The physical model is a system of partial differential equations accompanied by measured data. Jing [17] et al. performed a kidney surgery using VR in which a linear material model is used for the kidney. The major advantage of physics-based models is that one can obtain physically correct and interpretable results that are important for some engineering and medical applications. The disadvantage is that these methods are computationally challenging, fortunately, with the proposed domain decomposition method, the problems can be mapped and solved on supercomputers using a large number of processor cores.

In this paper, we propose and test a digital twin model based on a system of hyperelasticity equations to predict the motion and deformation of the four chambers of a human heart. As a pre-operative step, the patient's heart is scanned and the segmentation and reconstruction of a digital heart is obtained as an off-line procedure. The intended application of the platform is for the doctors to see the actual patient and the predicted changes of the heart at the same time via the holographic device with live data feeding from the digital twin. One can interact with the numerical simulation by changing some of its physical and geometrical parameters through some pre-defined hand gestures and actions.

Because of the recent advancement of supercomputing technologies, there has been a lot development of physics-based models of human organs [18] [19] [20]. The use of AR technologies in the operation room has also attracted a lot attention. Gibby [9] used AR with head-mounted display to guide pedicle screw placement. Judy [12] applied AR technology to assist an S2 Alar-Iliac screw placement surgery. They found that the overall accuracy is higher than freehand or robotic placement. There are many studies using AR or VR in cardiovascular care [11]. The users of such technologies are not limited to the doctor, but also the patient and educators.

The remainder of this paper is organized as follows. In Section 2, we introduce an interactive platform with a pair of holographic glasses, a hyperelasticity model of a human heart, and a parallel computer for the numerical solution of the physical model discretized by a finite element method. In Section 3, we present some preliminary results and experiences with a patient-specific heart. Some concluding remarks are given in Section 4.

II. An interactive platform for the digital twin of a human heart

In Fig. 1, we present the major components of an interactive platform with a pair of holographic glasses, a platform manager, a digital twin of a human heart, and a parallel computer cluster as the computational engine. More specifically, Fig. 1(a) shows the user with a pair of head mounted holographic glasses. The cameras on the glasses are able to view/capture both the virtual object (i.e., the digital heart) and certain hand gestures. Through the glasses the user can view both the digital and actual objects overlaying each other. Fig 1(b) is the main controller of the platform called the platform manager (PM). The information from the glasses is received by the PM who decides on the corresponding actions to be taken. If the action is to find, for example, the new shape of the heart due to the action of the user then the PM will send the command to the computational engine as shown in Fig 1(c). The computational results will then be sent back to the PM who will then send to the user's glasses. The PM is a GPU-based machine and the computational engine is built with CPUs. The connection between the holographic device and the PM is wireless, and between the PM and the computational engine is fiber optic.

A. Interaction with hologram

The interaction of the user with the digital heart is through the head mounted holographic device (Microsoft Hololens 2) with cameras to capture the user's gestures and glasses to see the digital and also the actual objects simultaneously. Only a small number of gestures are introduced for our current application. For example, the user can push or pull a small area on the surface of the heart, and the small deformation is felt by the whole heart. The initial push or pull is captured by the cameras and the global deformation of the heart is then calculated by the computational engine.

To make the use of the system more intuitive, the virtual hands are projected onto the real hands in the device, and we detect and record finger tips and knuckles. Some actions are defined, for example, tipping of the right thumb and the right forefinger triggers the action of pinching which captures the closest point on the object's surface. The motion of the points is communicated to the computational engine which makes use of such input data in the boundary conditions for solving

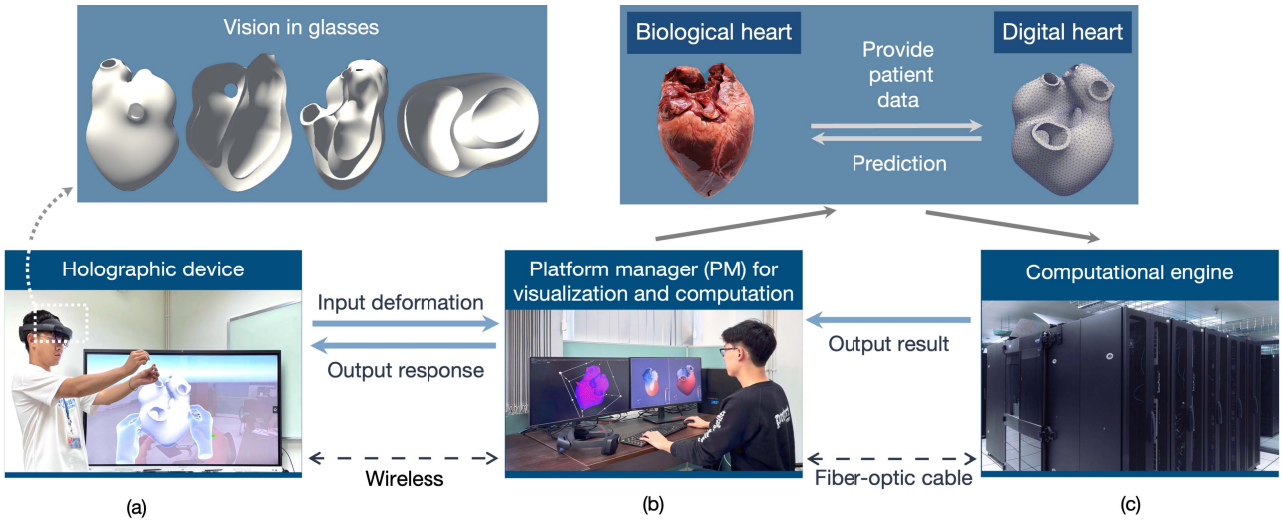

Fig. 1. The basic components of the proposed platform. (a) the holographic device with cameras and a pair of glasses; (b) the platform manager to receive data from the holographic device and to control the modeling running on the computational engine; (c) a parallel computer cluster to solve the large system of equations from the finite element discretization of the physical model of the heart. The top-left subfigure shows some views of the digital heart that the user can see in the glasses. These views are impossible to obtain for the live biological heart. The top-right subfigure shows that the PM may send live patient data to the computational engine.

a numerical elastic problem on a parallel computer. The results from the computational engine are sent back to the platform manager for further processing. The new shape of the digital heart can be viewed in the holographic glasses directly from any angle and any distance.

Ideally the process described above should happen in real time; in other words, the process starting from the time we touch a small area of the digital heart to the time we see the response of the whole heart should take as little time as possible. Since the holographic device is head mounted, its processing power and the amount of memory are both limited. To render the holograms as a time series of frames with very little latency between frames, the main rendering workhorse is a graphical workstation to be called the platform manager in the rest of the paper. Low-latency high-speed communication between the holographic device and the platform manager is vital. Transferring the gesture signal and the deformation data of the 3D digital heart in real time requires a bandwidth around 100Gbps∼2Tbps [21], which is often beyond the reach of most indoor wifi connection. Thus, in our platform only the surface part of the heart is rendered, and other interior cuts can also be handled if the user desires, but additional requests have to be sent to the manager.

B. Mathematical model of the digital heart

The geometry of a human heart is reconstructed from some high resolution CT images. Because of the geometric complexity of the heart, traditionally, this segmentation step requires enormous manual efforts to calibrate the differences of gray scales of the heart muscles with its surrounding tissues and the results are often not sufficiently accurate. The recent development of machine learning technique provides a powerful tool to overcome this difficulty [22] [23]. With a deep neural network based method for training, we are able to reconstruct the 3D geometry of a four-chamber heart with sufficient accuracy to test the platform proposed in this paper. Fig. 2 shows the 3 basic steps including the scanning of the patient, the image segmentation of the 2D slides of the images, and the construction of the full 3D geometry of the heart.

Based on the geometry of the heart, we next create an unstructured conformal finite element mesh for the purposes of numerical modeling, visualization, and interactive control of the simulation. Physical quantities of interest, such as the deformation of the heart, are computed by solving a partial differential equation discretized on the mesh.

The dynamic of the heart under the action of external force reflects the inherent elastic mechanics of cardiac tissue. We consider the Saint-Venant-Kirchhoff model to describe the elastic deformation of the heart in this digital twin. Let Ω be the domain of the heart, $\partial\Omega$ be its surface, and $\bar{\Omega} = \Omega \cup \partial\Omega$. We denote $u(x, y, z, t)$ as the displacement of the heart which is governed by the following PDEs:

$$\nabla \cdot \sigma^T + g = \rho \frac{\partial^2 u}{\partial t^2}, \quad (x, y, z) \in \Omega, t \in (0, T], \tag{II.1}$$

$$\sigma = \lambda tr(\varepsilon) I + 2\mu\varepsilon, \tag{II.2}$$

$$\varepsilon = \frac{1}{2}\left[\nabla u + (\nabla u)^T + (\nabla u)^T(\nabla u)\right], \tag{II.3}$$

with initial and boundary conditions:

$$u = u_d, \quad (x, y, z) \in \Gamma_d, t \in (0, T], \tag{II.4}$$

$$\sigma \cdot n = u_n, \quad (x, y, z) \in \partial\Omega \backslash \Gamma_d, t \in (0, T], \tag{II.5}$$

$$u(x, y, z, 0) = u_0, \quad (x, y, z) \in \bar{\Omega}. \tag{II.6}$$

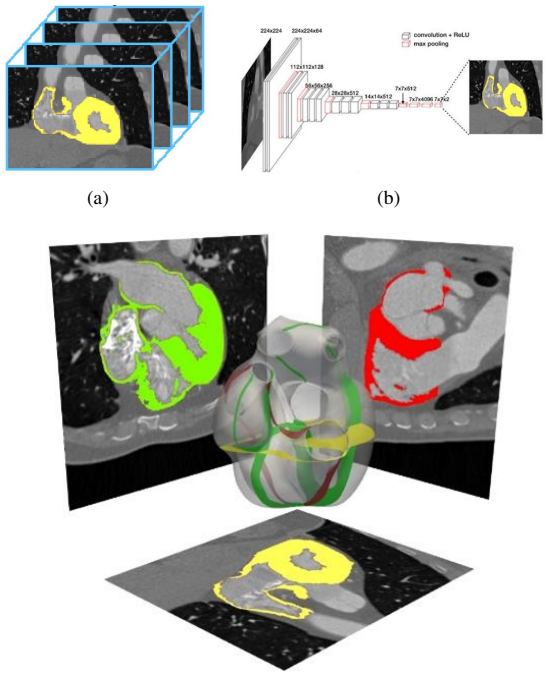

(a) (b) (c)

Fig. 2. (a) Slides of original 2D CT images, in which the muscles of the heart are highlighted in yellow, (b) Image segmentation of the heart muscles using DNN, and (c) reconstructed 3D geometry of the heart with four chambers and its projection to the three coordinate directions.

Here Γ_d is part of the surface with the Dirichlet boundary condition. $(0, T]$ is the time period of the simulation, and in this particular case, it is one cardiac cycle. n is the unit outward normal vector of the surface. σ is the stress tensor and ε is the strain tensor. The trace operator $tr(\cdot)$ is the summation of the diagonal elements of the matrix it applied which is $tr(\varepsilon) = \varepsilon_{11} + \varepsilon_{22} + \varepsilon_{33}$. $g(x, y, z, t)$ is the body force on the material. $u_d(x, y, z, t)$ is the given displacement on Γ_d, $u_n(x, y, z, t)$ is the traction force acting on $\partial\Omega\backslash\Gamma_d$, and $u_0(x, y, z)$ is the initial displacement in $\bar{\Omega}$. ρ is the density of the material. μ and λ are the Lamé parameters of the elastic material. Two important parameters are the Young's modulus $E = \frac{\mu(3\lambda+2\mu)}{\lambda+\mu}$ describing the resistance of the material to the deformation, and the Poisson's ratio, $\nu = \frac{\lambda}{2(\lambda+\mu)}$, defined as the ratio of the transverse strain to axial strain. We use a finite element method for the spatial discretization of (II.1)-(II.6) on a fully unstructured mesh and a generalized-α method for the temporal discretization. Note that (II.1)-(II.6) is a nonlinear model and a linear model is also provided in our system.

A prestress process is applied to calculate the instantaneous displacement with the user's input as the Dirichlet boundary conditions. To obtain a sufficiently accurate simulation, the required finite element mesh is rather large, and the corresponding computation needs to be carried out on a large-scale parallel computer. In the proposed platform we ship this computational task to a computer cluster connected directly to the platform manager. A scalable algorithm is used to reduce the computing time linearly as we increase the number of processor cores of the cluster.

C. A linearly scalable method for the hyperelastic heart model

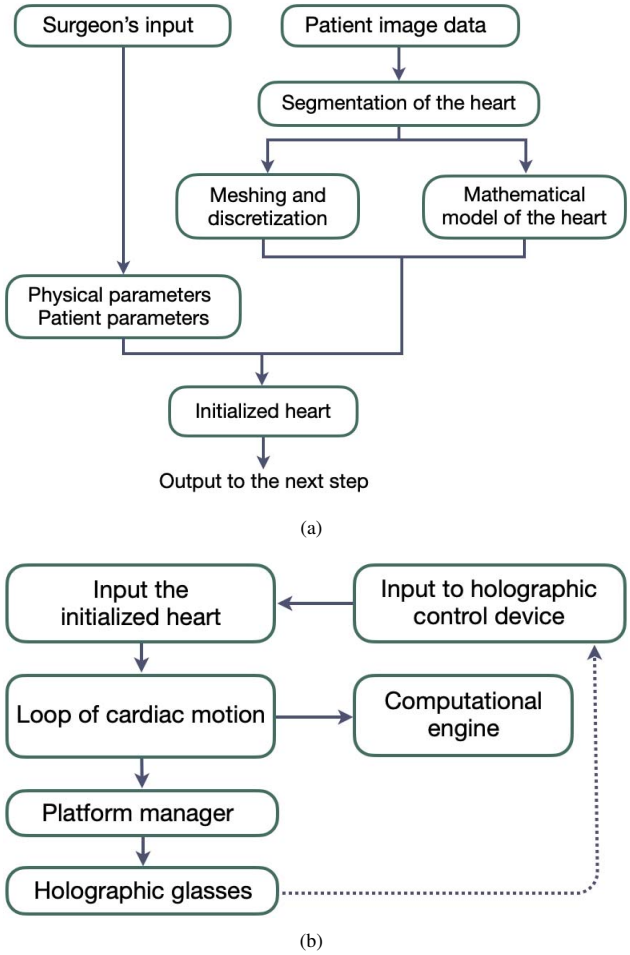

Fig. 3. (a) Basic steps to prepare the digital model for the real-time application. All steps are computed off-line; (b) Real-time simulations with pre-built model and interactive gesture control.

The detail of the building process of the digital twin of the human heart is shown in Fig. 3. The process can be divided into phases. The first phase is the initialization of the digital heart, and this step doesn't need to be carried out in real time. As shown in Fig. 3(a) the patient data is loaded to the platform, this includes the image data, and some physical parameters. An image segmentation is performed with some standard denoising and smoothing. Then a finite element mesh is created, and also partitioned into submeshes for the purpose for parallel processing as shown in Fig 4. Moreover, the subdomain matrices are also pre-factorized in order to be used as the preconditioner in the numerical solver.

The second phase, as shown in Fig. 3(b), needs to be performed in as close to real time as possible. In this phase,

the initialized heart is loaded to the holographic device. The input is used to setup the boundary condition, then the cardiac motion is activated and interactively controlled by the user's hand gestures obtained by the platform manager from the holographic glasses.

The general discretized, nonlinear model of human heart can be written in the form of a large, sparse, nonlinear algebraic system of equations for each time step:

$$F^n(U^n) = 0, \tag{II.7}$$

where F^n denotes the discretized nonlinear operator and U^n represents the interested physical fields, such as displacement, strain, velocity, and pressure [24]. To proceed, (II.7) is solved by using a Newton-Krylov-Schwarz (NKS) algorithm [25] [15] [18] [19], in which the Jacobian matrix J^n of F^n and a restricted additive Schwarz (RAS) preconditioning matrix M^{-1} need to be constructed. In particular, J is defined by

$$J^n = \nabla F^n(U^n) = \frac{\partial F^n}{\partial U^n}, \tag{II.8}$$

and M^{-1} is a good approximation of the inverse of J^n and can be cheaply calculated through a domain decomposition method. The NKS algorithm has been verified to be highly effective and highly scalable for many engineering applications, and serves as the key ingredient for our digital twin model to achieve efficient real-time simulations.

Algorithm 1 An implicit time-stepping Newton-Krylov-Schwarz algorithm for solving the discretized model of the heart.

1: Set U^0 according to the initial condition.
2: **for** time step $n = 1, 2, \ldots, N$. **do**
3: Let $U^n_m = U^{n-1}$ as $m = 0$, compute $F = F^n(U^n_0)$.
4: **while** $\|F\|$ is too large **do**
5: Calculate the Jacobian matrix

$$J = J^n(U^n_m) = \nabla F^n(U^n_m), \tag{II.9}$$

and construct the RAS preconditioner M^{-1}.
6: Use the GMRES method to solve the right-preconditioned system

$$(JM^{-1})(M\Delta U) = -F, \tag{II.10}$$

inexactly for an approximate solution ΔU.
7: Find α via a line search method.
8: Update $U^n_{m+1} = U^n_m + \alpha\Delta U$, let $m = m + 1$, and compute $F = F^n(U^n_m)$.
9: **end while**
10: Set $U^n = U^n_m$ as the solution of the current time step.
11: **end for**

Two most important factors that affect the efficacy and efficiency of the NKS algorithm are the construction of J and M^{-1}. Traditionally, J is often computed through a finite difference approximation that involves massive evaluations of the nonlinear function F with small perturbations on the input vector U. Although it is easy to program, this approach

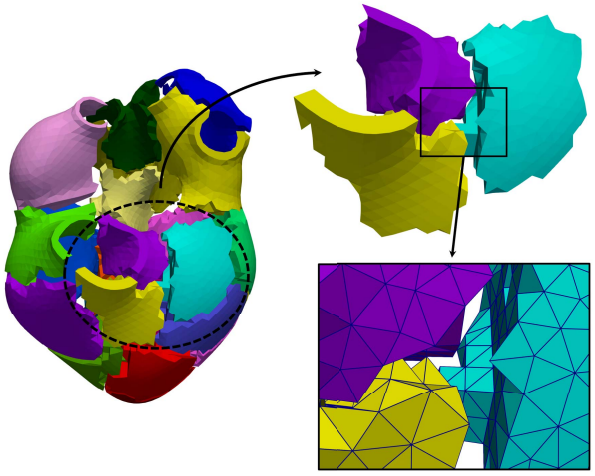

Fig. 4. A partition of a heart mesh into 24 subdomains. Each color represents a different subdomain and subproblems defined on different subdomains are solved concurrently using the computational engine.

is very time consuming and has a relatively low stability. In this work, the Jacobian matrix is constructed according to its analytic form, and the RAS preconditioner M^{-1} is constructed based on a partition of the problem domain (see Fig. 4 for an example), which suits naturally the architecture of a parallel computer that consists of many processor cores with distributed memories. In such a circumstance, each core is allocated a part of the mesh, and responsible for computations and data communications that relate to the subdomain. M^{-1} can be written by in the following matrix form:

$$M^{-1} = \sum_{i=1}^{n_p} (R_i^0)^T J_i^{-1} R_i^\delta, \tag{II.11}$$

where n_p denotes the total number of subdomains in this mesh partition, R_i^0 and R_i^δ are two restriction operators that component-wisely reduce a global vector U to the i-th subdomain and its extension with δ layer of cells, respectively. The transposes of R_i^0 and R_i^δ are the corresponding prolongation operators from the related subdomains to the whole domain, and J_i^{-1} represents a linear solve to produce an approximate solution of the subdomain problem that is constructed by restricting the original linear system (i.e., the Jacobian system) onto the extended subdomain.

III. Result

In this section, we present an example to illustrate how the proposed framework works. First, the 3D geometric model of the heart of a patient is reconstructed from the CT images. Then, a finite element mesh with tetrahedral elements is generated. For this particular test, we use a mesh with 55686 tetrahedrons and 12194 points. The surface mesh has 18099 triangles and 5738 points. For the purpose of parallel processing, the mesh is partitioned into subdomains (see Fig. 4) and the subproblems defined on subdomains are mapped to

different processors of the computational engine and solved concurrently.

After starting the interactive mode of the platform, the surface mesh of the heart is loaded to the platform manager for visualization and computation and the volumetric mesh of the heart is loaded to the computational engine. Some pre-operative computations are carried out including the partition of the mesh into submeshes according to the number of processor cores requested on the computational engine, the incomplete factorization of the subdomain preconditioners to be used in the RAS calculations, and the pre-stress of the problem. Note that the pre-operative calculations are carried out off-line as a preparation step to the real-time application of the platform.

The interactive operations are controlled by the hand gestures first captured by the holographic device, then sent to the PM. There are several hand gestures that can be recognized by the system and the corresponding actions are performed by the PM. For example, the right hand pinch, which determines the location of a point is realized if the distance of the tip of the thumb and the tip of the forefinger is smaller than 1.0mm. As shown in Fig. 5, the finger tips are represented by small balls. When these two balls coincide with each other, it indicates that the finger tips touch each other and the action of a pinch is triggered.

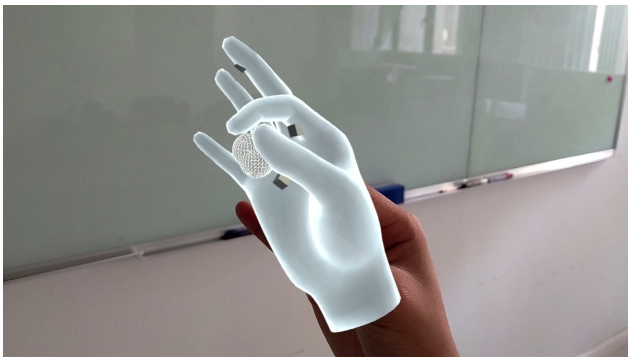

Fig. 5. A hand gesture to locate a particular point in space. This is realized by the touch of the tips of the thumb and the forefinger. The visual and the actual hands coincide each other in the glasses, but not in the above figure which is taken with the camera mounted on the top of the glasses in a location that is higher than the level of the eyes.

In the current implementation of the platform, we only consider points on the surface of the heart. With the pinch operation, any points of interests can be moved to a different locations and the coordinates are then recorded as an array for the surface displacement. This array is calculated and stored by the PM, and is to be used to determine the displacement of all interior points of the heart. Fig. 6 shows that the user picks a point with the pinch gesture on the visual heart from a third person perspective (a) and a first person perspective (b). Since the surface is represented by a finite element mesh, this operation is also realized by the finite element basic functions defined on triangles; in other words, the movement of a node of a triangle moves the entire triangle.

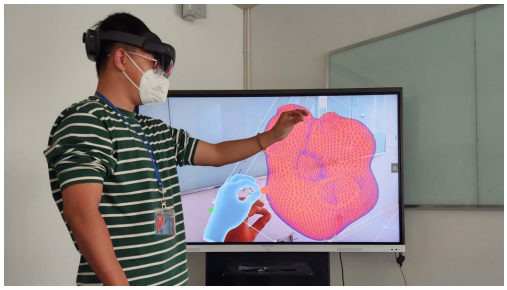

(a)

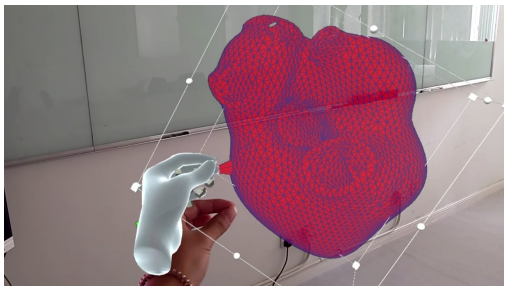

(b)

Fig. 6. Because the camera on the glasses is higher than the human eyes, the visual hand doesn't exactly overlay the human hand. (a) View of the hand gesture from a third person perspective, (b) View of the hand gesture from a first person perspective.

After the user finishing the manipulation of the surface of the digital heart with hand gestures, another gesture is used to start the calculation of the interior deformation of the heart in the computational engine. This gesture is defined as the touch of the tips of the right thumb with the left thumb. When this gesture is detected, the deformation array is sent to the computational engine by the PM. It is important to note that the total number of points displaced by the user is much smaller than the total number of points on the surface of the heart while the latter is also much smaller than the total number of interior points of the heart. The numbers of points in different parts determine the communication costs at different stages of the operation. Wireless communication between the glasses and the PM offers a reasonable solution, but the communication between the platform manager and the computational engine requires a fiber optic connection because of the amount of the data is much larger.

Once the user input is obtained by the computational engine, the surface deformation is extended to the interior of the heart, and this is done by solving (II.1)-(II.6) using the surface data as the boundary conditions. After the calculation, all the results are sent to the PM. More specifically, we consider the inferior vena cava cut as the Dirichlet boundary condition, and these mesh points manipulated by the user are set as Dirichlet boundary condition in the initial volumetric displacement calculation but in the subsequent time steps, they are treated as zero Neumann boundary conditions to represent free motion. In this simulation, (II.1)-(II.3) with initial condition (II.6) and boundary condition (II.4)-(II.5) is solved using the following

set of parameters. In the hyperelasticity material model, the Young's modulus is 10^{-3}Gpa, the Poisson's ratio is 0.25. In the inexact Newton method for solving the nonlinear system, the relative stopping condition is 10^{-6}. GMRES is used for solving the linear system with a relative tolerance 10^{-4} and an absolute tolerance 10^{-6}. RAS preconditioner is used with subdomain solver ILU(1). PETSc [26] is used for the linear and nonlinear algebraic solvers and for the mesh management.

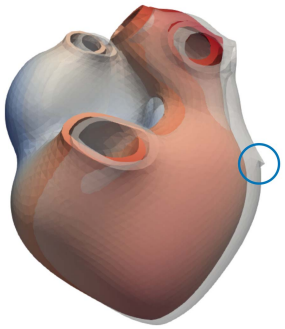

Fig. 7. The deformation of the digital heart from $t = 0$ (gray) to $t = 0.5$ (red). The circle represents a point displaced by the user.

In Fig. 7, we show the results of the calculation for about half of a cardiac cycle, that is from $t = 0$ to $t = 0.5$ since the heart rate is normalized to 1 second. The gray image shows the initial shape of the heart, and the red image shows the shape at $t = 0.5$. Note that the user only touched a small surface area of the heart, but the entire heart changes. This simulates, for example, an important condition of the heart, namely certain problem that happens to a small number of cells may impact the entire myocardium. It is important to note that with a biological heart one can only see a small portion of the surface of the heart during an actual operation, but with a digital heart one can see the entire heart, including the entire outer surface and surfaces of the ventricles, as well as any cross sections. In the top-left subfigure of Fig 1, we show several views of the digital heart that are extremely valuable to the heart surgeon as 3D images (still frames) or as 4D images (videos) during the operation.

In Fig. 8, we show the time history of the displacement for several points on the heart as marked by A, B, C, and D. "A" is the point where the user initializes the movement. As expected, the movement of the points are truly three dimensional (i.e., not on a line or on a plane). The actual space-time path of the points are valuable information about the health of the heart. We remark that in this paper, we only consider the displacement of the heart muscles, but there are many other aspects of the heart that can be studied using the proposed platform such as the electric system of the heart, and the dynamics of the blood flows in the heart.

Next, let us look at the performance of the proposed platform in terms of the communication and computational times. Since we have not attempted to optimize the hardware, the network, and the software implementation, the recorded times in the following discussion are larger than expected.

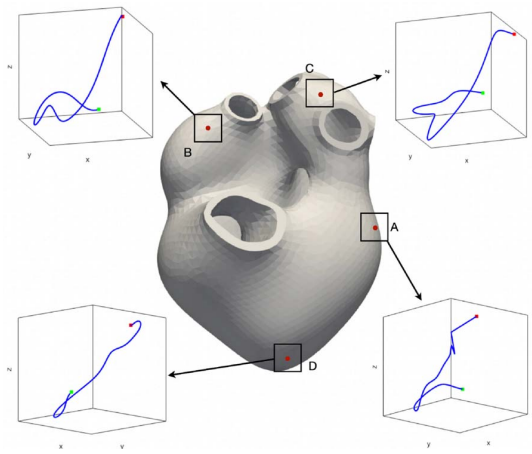

Fig. 8. The space-time trajectories for 4 points on the heart are shown for a cardiac cycle. Point A is where the user touches initially.

There are 3 computational tasks: (l) rendering the frames of holograms and virtual hands by the CPU in the holographic device, (2) recognizing the hand gestures and manipulating of the heart surface by the PM, and (3) evaluating the deformation of the interior of the digital heart by the computational engine. Tasks (1) and (2) cost about 0.02s for handling 1 frame on average. Task (3) takes 17.52s when using 16 processor cores. This is by far the dominate component of the overall time because the mesh is selected to offer realistic displacement of a patient-specific heart.

There are two types of data communication. The amount of data traveling between the holographic device and the PM is rather small, and depending on the latency of the wireless network, in our tests, the time is often around 0.1s. The data traffic between the PM and the computational engine is a little larger. For our tests, it takes about 0.28s to send data to the computational engine, and 0.86s to send data back to the PM. Some optimization to reduce the communication cost can be performed, but have yet to be considered in the current implementation such as data compression and the use of the single precision data type.

We observe that the current performance bottleneck, for this test case, comes from the numerical solver on the computational engine with a relatively small number of processor cores. Note that one of the important capabilities of the proposed computational engine is its scalability. Depending on the requirements of the applications, the accuracy can be increased by using a finer finite element mesh, and the computational time can be reduced by increasing the number of processor cores. In Table I, we show results for computations carried out with two different meshes, one with around 56,000 elements and another with around 445,000 elements. The number of processor cores range from 32 to 256. For the smaller mesh, the total compute time is about 4.31s.

IV. Conclusion

In this paper, we developed and tested an interactive plat-

TABLE I
PARALLEL SCALABILITY OF THE NKS ALGORITHM FOR SOLVING THE NONLINEAR ELASTODYNAMIC PROBLEM ON TWO MESHES.

	Mesh 1 (56K elem.)	Mesh 2 (445K elem.)
# Cores	Time (s)	Time (s)
32	14.92	103.77
64	10.87	65.61
128	6.58	43.39
256	4.31	28.53

form for a high performance digital twin of a realistic human heart with four chambers, and the platform consists of a pair of holographical glasses with cameras to record the user's hand gestures to be used to control the overall computation, a high-end graphical workstation as the platform manager to render the data and control the computations, and a high performance computer cluster to handle the large-scale computations required by the physics-based model of the heart. Through the holographical glasses, the user is able to view both the physical and the digital object simultaneously, and at the same time to manipulate the digital object using pre-defined hand gestures. There are many possible applications of the system such as surgical planning as an off-line process, or a near real-time tool during certain operations. To reduce the times spent in various communication and computational steps is necessary in order to allow more complex gesture controls and more accurate physical models of the object. The extension to multiple users each with a pair of holographic glasses is possible but will increase the complex of the platform considerably. The subsystem Fig. 1(a)+(b) without the computational engine is also of great value in certain applications when the digital twin is pre-computed and stored.

REFERENCES

[1] J.-S. Kang, K. Chung, and E. J. Hong, "Multimedia knowledge based bridge health monitoring using digital twin," *Multimedia Tools and Applications*, vol. 80, no. 26, pp. 34 609–34 624, 2021.

[2] A. McClellan, J. Lorenzetti, M. Pavone, and C. Farhat, "A physics-based digital twin for model predictive control of autonomous unmanned aerial vehicle landing," *Philosophical Transactions of the Royal Society A: Mathematical, Physical and Engineering Sciences*, vol. 380, no. 2229, p. 20210204, 2022.

[3] M. G. Kapteyn, D. J. Knezevic, D. Huynh, M. Tran, and K. Willcox, "Data-driven physics-based digital twins via a library of component-based reduced-order models," *International Journal for Numerical Methods in Engineering*, vol. 123, no. 13, pp. 2986–3003, 2022.

[4] T. Ritto and F. Rochinha, "Digital twin, physics-based model, and machine learning applied to damage detection in structures," *Mechanical Systems and Signal Processing*, vol. 155, p. 107614, 2021.

[5] B. J. Park, S. J. Hunt, G. J. Nadolski, and T. P. Gade, "Augmented reality improves procedural efficiency and reduces radiation dose for CT-guided lesion targeting: a phantom study using HoloLens 2," *Scientific Reports*, vol. 10, no. 1, p. 18620, 2020.

[6] M. G. Hanna, I. Ahmed, J. Nine, S. Prajapati, and L. Pantanowitz, "Augmented reality technology using Microsoft HoloLens in anatomic pathology," *Archives of Pathology Laboratory Medicine*, vol. 142, no. 5, pp. 638–644, 2018.

[7] J. Jang, C. M. Tschabrunn, M. Barkagan, E. Anter, B. Menze, and R. Nezafat, "Three-dimensional holographic visualization of high-resolution myocardial scar on hololens," *PLOS ONE*, vol. 13, no. 10, pp. 1–14, 2018.

[8] S. Zafar and J. J. Zachar, "Evaluation of HoloHuman augmented reality application as a novel educational tool in dentistry," *European Journal of Dental Education*, vol. 24, no. 2, pp. 259–265, 2020.

[9] J. T. Gibby, S. A. Swenson, S. Cvetko, R. Rao, and R. Javan, "Head-mounted display augmented reality to guide pedicle screw placement utilizing computed tomography," *International Journal of Computer Assisted Radiology and Surgery*, vol. 14, no. 3, pp. 525–535, 2019.

[10] A. A. Rad, R. Vardanyan, A. Lopuszko, C. Alt, I. Stoffels, B. Schmack, A. Ruhparwar, K. Zhigalov, A. Zubarevich, and A. Weymann, "Virtual and augmented reality in cardiac surgery," *Brazilian Journal of Cardiovascular Surgery*, vol. 37, no. 01, pp. 123–127, 2022.

[11] C. Jung, G. Wolff, B. Wernly, R. R. Bruno, M. Franz, P. C. Schulze, J. N. A. Silva, J. R. Silva, D. L. Bhatt, and M. Kelm, "Virtual and augmented reality in cardiovascular care," *JACC: Cardiovascular Imaging*, vol. 15, no. 3, pp. 519–532, 2022. [Online]. Available: https://www.jacc.org/doi/abs/10.1016/j.jcmg.2021.08.017

[12] B. F. Judy, A. Liu, Y. Jin, C. Ronkon, M. Khan, E. Cottrill, J. Ehresman, Z. Pennington, A. Bydon, S.-F. L. Lo *et al.*, "In-human report of S2 alar-iliac screw placement using augmented reality assistance," *Operative Neurosurgery*, pp. 10–1227, 2023.

[13] J. Cartucho, D. Shapira, H. Ashrafian, and S. Giannarou, "Multimodal mixed reality visualisation for intraoperative surgical guidance," *International Journal of Computer Assisted Radiology and Surgery*, vol. 15, no. 5, pp. 819–826, 2020.

[14] B. Sevim, A. Bayraktar, A. C. Altuniik, S. Atamtrktr, and F. Birinci, "Finite element model calibration effects on the earthquake response of masonry arch bridges," *Finite Elements in Analysis and Design*, vol. 47, no. 7, pp. 621–634, 2011.

[15] Y. Jiang, R. Chen, and X.-C. Cai, "A highly parallel implicit domain decomposition method for the simulation of the left ventricle on unstructured meshes," *Computational Mechanics*, vol. 66, no. 6, pp. 1461–1475, 2020.

[16] E. R. Conde López, M. Á. Toledo, and E. Salete Casino, "Optimization of numerical models through instrumentation data integration: Digital twin models for dams," *Computational and Mathematical Methods*, vol. 3, no. 6, p. e1205, 2021.

[17] M. Jing, Z. Cui, H. Fu, and X. Chen, "Real-time deformation simulation of kidney surgery based on virtual reality," *Journal of Shanghai Jiaotong University (Science)*, vol. 26, no. 3, pp. 290–297, 2021.

[18] S. Qin, R. Chen, B. Wu, and X.-C. Cai, "A highly parallel fully implicit domain decomposition method for the simulation of the hemodynamics of a patient-specific artery at the full-body scale," *Journal of Computational Physics*, vol. 472, p. 111730, 2023.

[19] Z. Yan, Z. Yao, W. Guo, D. Shang, R. Chen, J. Liu, X.-C. Cai, and J. Ge, "Impact of pressure wire on fractional flow reserve and hemodynamics of the coronary arteries: A computational and clinical study," *IEEE Transactions on Biomedical Engineering*, pp. 1–9, 2022.

[20] W. Ma and X.-C. Cai, "Point-block incomplete LU preconditioning with asynchronous iterations on GPU for multiphysics problems," *The International Journal of High Performance Computing Applications*, vol. 35, no. 2, pp. 121–135, 2021.

[21] A. Clemm, M. T. Vega, H. K. Ravuri, T. Wauters, and F. D. Turck, "Toward truly immersive holographic-type communication: challenges and solutions," *IEEE Communications Magazine*, vol. 58, no. 1, pp. 93–99, 2020.

[22] L. Gu and X.-C. Cai, "Fusing 2D and 3D convolutional neural networks for the segmentation of aorta and coronary arteries from CT images," *Artificial Intelligence in Medicine*, vol. 121, p. 102189, 2021.

[23] L. Gu, W. Zhang, J. Liu, and X.-C. Cai, "Decomposition and composition of deep convolutional neural networks and training acceleration via sub-network transfer learning," *Electronic Transactions on Numerical Analysis*, vol. 56, pp. 157–186, 2022.

[24] A. Bertram, *Elasticity and Plasticity of Large D eformations*. Springer, 2012.

[25] L. Luo, W.-S. Shiu, R. Chen, and X.-C. Cai, "A nonlinear elimination preconditioned inexact newton method for blood flow problems in human artery with stenosis," *Journal of Computational Physics*, vol. 399, p. 108926, 2019.

[26] S. Balay, S. Abhyankar, M. F. Adams, S. Benson, J. Brown, P. Brune, K. Buschelman, E. M. Constantinescu, L. Dalcin, A. Dener, V. Eijkhout, J. Faibussowitsch, W. D. Gropp, V. Hapla, T. Isaac, P. Jolivet, D. Karpeev, D. Kaushik, M. G. Knepley, F. Kong, S. Kruger, D. A. May, L. C. McInnes, R. T. Mills, L. Mitchell, T. Munson, J. E. Roman, K. Rupp, P. Sanan, J. Sarich, B. F. Smith, S. Zampini, H. Zhang, H. Zhang, and J. Zhang, "PETSc," 2023.